Energy-efficient CuO/TiO_2@GCN cellulose acetate-based membrane for concurrent filtration and photodegradation of ketoprofen in drinking and groundwater

Lethula E. Mofokeng [1,2], Lerato Hlekelele [1], John Moma [2], Zikhona N. Tetana [3,4], Vongani P. Chauke [1*]

[1] Council for scientific and industrial research,
Meiring Naude Road, Brummeria, Pretoria, 0184, South Africa.
[2] Molecular Sciences Institute, School of Chemistry, University of the Witwatersrand, Private Bag X3, Johannesburg, 2050, South Africa.
[3] DST-NRF Centre of Excellence in Strong Materials, University of the Witwatersrand, Johannesburg, 2050, South Africa.
[4] Microscopy and Microanalysis Unit, University of the Witwatersrand, Private Bag 3, 2050, Johannesburg, South Africa

*Correspondence email: VChauke@csir.co.za

S1

Preparation of TiO_2 nanoparticles.

Typically, TTIP (3mL) was added into 2-propanol (50mL) while magnetically stirring for 10 min to form a uniform solution. Concentrated HNO_3 (0.15 mL) was added into the TTIP solution while stirring continuously for further a 30 min to assist hydrolysis of the TTIP precursors. Tri-potassium citrate (1 mmol) was dissolved separately in deionized water (10 mL) and added into a TTIP mixture. The mixture was magnetically stirred for 4 h at room temperature and aged for 12 h to allow the growth of the crystals. After gelation, the obtained gel was centrifuged, washed with deionized water and ethanol several times, and dried at 85 °C for 12 h in a vacuum oven. The dried product was ground into fine powders using pestle and mortar and finally calcined in a muffle furnace at 450 °C for 4 h in the air at a rate of 10 °C/min to obtain whitish TiO_2.

S2

Preparation of CuO/TiO_2 photocatalysts

CuO doped TiO_2 nanoparticles were fabricated using the wet impregnation method adopted in the previous literature with minor modifications [44]. Typically, $CuSO_4.5H_2O$ weights (0.1 g, 0.2 g, and 0.4 g) were dissolved in deionized water (100 mL) and TiO_2 (1 g) was added. The Ti-Cu mixtures were stirred magnetically for 4 h and heated for 2 h at 75 °C using a hot plate. The obtained particles were centrifuged, washed several times with deionized water and ethanol to remove impurities. The obtained particles were dried in a vacuum oven for 12 h at 85 °C. The dried particles were ground using pestle and mortar into fine powders. Thereafter, the particles were calcined for 4 h in the air at 450 °C at the rate of 10 °C/min using a muffle furnace to obtain CuO/TiO_2.

S3

Preparation of graphitic carbon nitride

Typically, 6 g of melamine was placed in a covered ceramic crucible to avoid melamine being combusted into the air and heated in a muffle furnace at 550 °C for 4 h at the rate of 10 °C/min. After cooling down at room temperature, the yellowish bulk graphitic carbon nitride was ground with pestle and mortar to fine yellowish powders. Finally, 0.5 g of bulk graphitic carbon nitride was heated further using an open ceramic crucible to form thermally exfoliated sheets of graphitic carbon nitride at 525 °C for 2 h at the rate of 3 °C/min in a muffle furnace. After calcination cooled down, the exfoliated graphitic carbon nitride sheets were denoted as GCN.

S4

Preparation of cellulose acetate membranes

Typically, 15 g of CA powder was dissolved in DMSO (85 mL) at 60 °C for 6 h to form a homogenous casting solution. Thereafter, the mixture was degassed for 12 h and then, scattered on the glass plate using a casting knife (150 µm) and immersed instantly in a deionized water bath to remove DMSO residues. The wet membranes were retained and transferred into a freshwater bath filled with deionized water for 24 h to ensure complete phase separation. The as-prepared membranes were taped on the glass plate and dried at room temperature.

S5

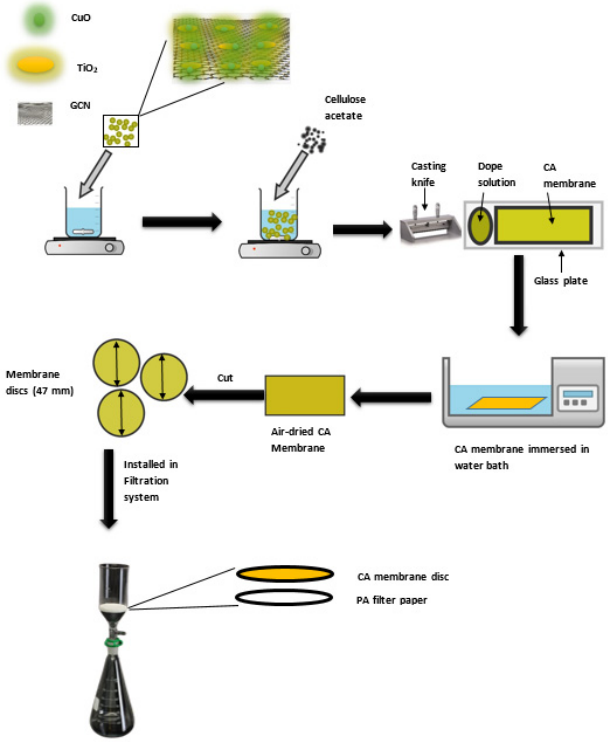

Figure S1. Systematic illustration for the fabrication of CA-based membranes embedded with ternary 1% CuO/TiO_2@GCN (1:9) nanocomposite.

S6

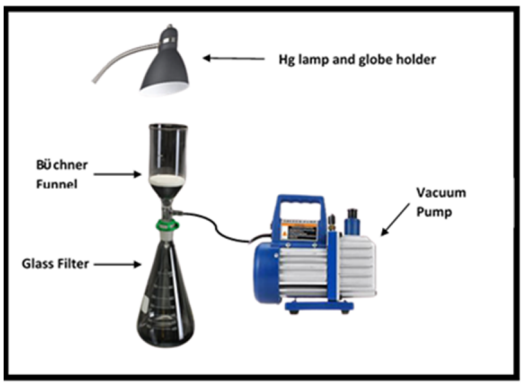

Figure S2. Filtration setup equipped with a medium power mercury lamp (165W) and vacuum pump (100W).

S7

TEM and SEM analysis of 1% CuO/TiO_2@GCN nanocomposite

Figure S3 are the (**a**) TEM and (**b**) SEM images of the photocatalyst, i.e. 1% CuO/TiO_2. Here, it was observed that the nanocomposite consists of granular like nanoparticles that are agglomerated together. The size of the 1% CuO/TiO_2 nanocomposites was determined by Sherrer's equation and were found to be 18 nm. The EDX spectrum of 1% CuO/TiO2 nancomposite confirmed that the material consists Cu, O and Ti. **Figure S3d** exhibits the clustered TEM image of 1% CuO/TiO_2@GCN (1:9) nanocomposite with the tail marks of CuO/TiO_2 spread randomly along with the GCN sheets. SEM image in **Figure S3e** shows 1% CuO/TiO_2 nanoparticles on the surfaces of GCN. SEM elemental mapping in **Figure S3(f, g, h and i)** provided evidence of the presence of key elemental compositions in 1% CuO/TiO_2@GCN (1:9) nanocomposite such as Cu, Ti, O, and C, which emanated from CuO/TiO_2 and GCN, respectively. EDX spectrum in **Figure S3j** confirmed that elemental components, Cu, Ti, and O, which were attributed to CuO/TiO_2 were supported successfully on the surfaces of GCN.

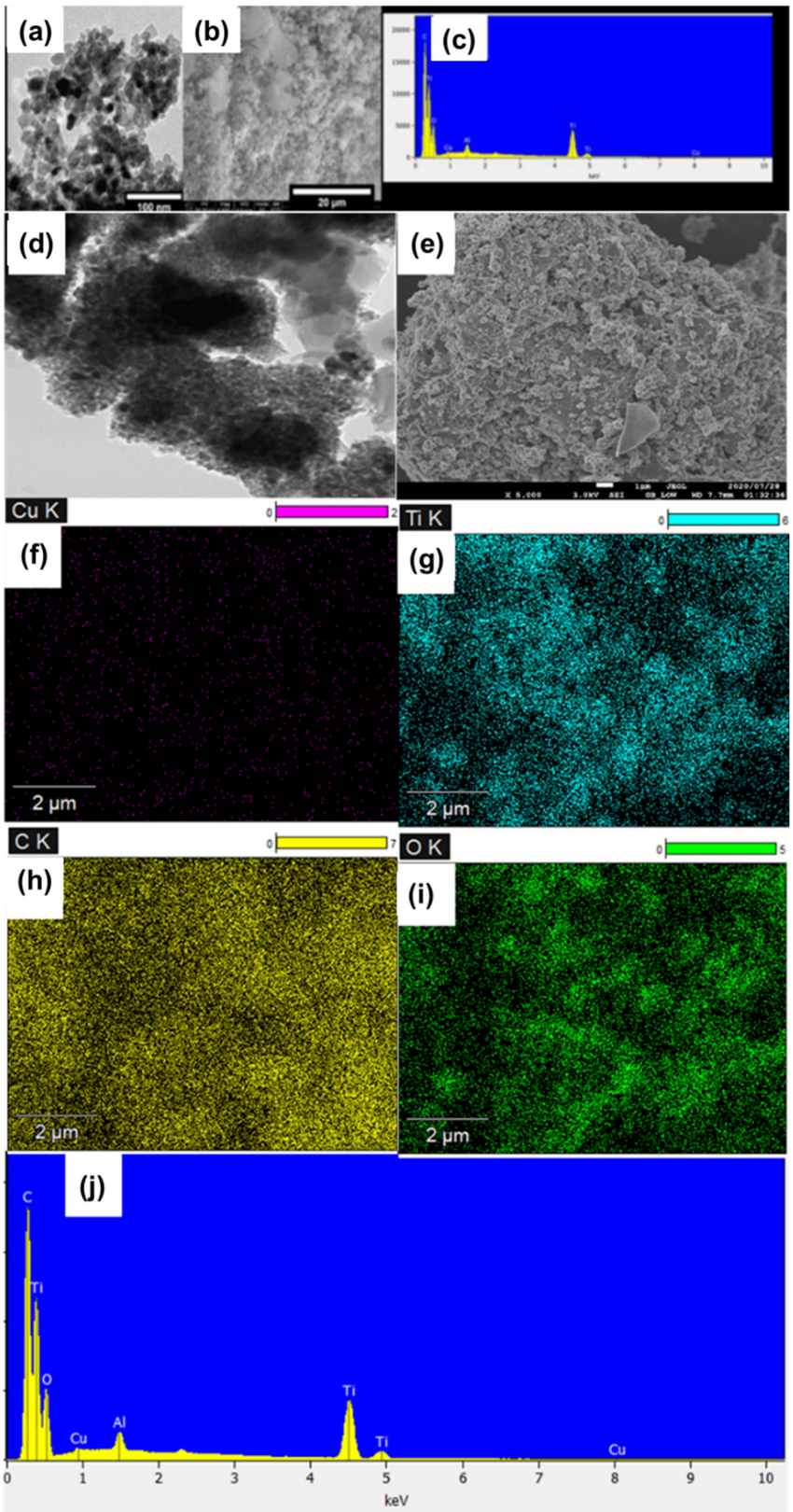

Figure S3. TEM images of (**a**) 1% CuO/TiO_2 and (**d**) 1% CuO/TiO_2@GCN (1:9) nanocomposite, SEM images of (**b**) TiO_2 and (**e**) of 1% CuO/TiO_2@GCN (1:9) nanocomposite, EDX spectrum of (**c**) 1% CuO/TiO_2@GCN (1:9) nanocomposite and SEM elemental mapping of (**f**) Cu, (**g**) Ti, (**h**) C, and (**f**) O.

S8

Optical properties

The optical properties of a pure TiO_2, 1% CuO/TiO_2@GCN (1:9) nanocomposite was analyzed using UV/Vis in a range from 200 to 1100 nm. **Figure S4a** shows a hump-shaped TiO_2 peak appearing between 300 and 375 nm corresponding to the bandgap of 3.2 eV (**Figure S4b**). The impregnation of CuO onto TiO_2 embedded on GCN altered the absorption characteristics by showing broadened peaks extending into visible range wavelengths in **Figure S4a** with the estimated bandgap of 1.78 eV as observed in **Figure S4b.** This shifting of the absorption band of 1% CuO/TiO_2@GCN (1:9) was ascribed to the movement of charges from the valence band of CuO to the conduction band. Moreover, the d-d transitions of the Cu^{2+} ions tend to extend the absorption system of 1% CuO/TiO_2/GCN into higher wavelengths compared to undoped TiO_2 [1].

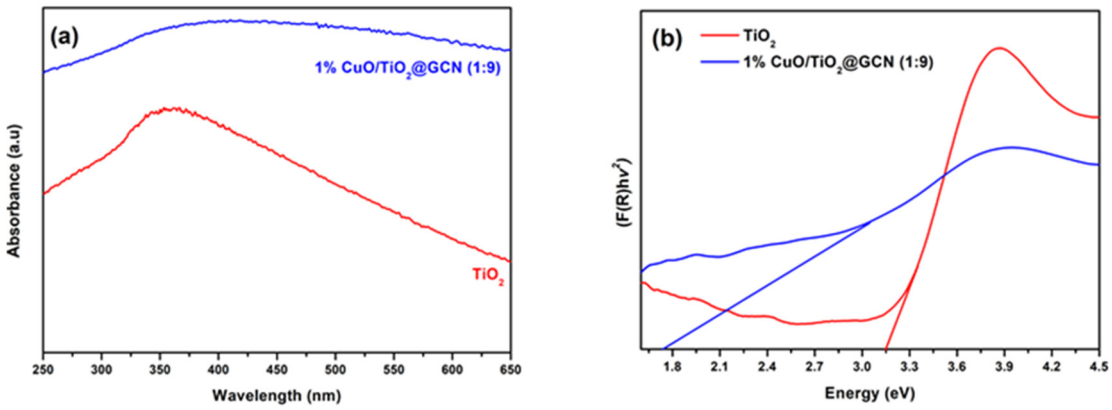

Figure S4. UV/Vis spectra of (**a**) unmodified TiO_2 and 1% CuO/TiO_2@GCN (1:9) nanocomposite and (**b**) their extrapolated energy bandgaps based on Kubelka-Munk method.

S9

Membrane properties

The as-prepared membranes porosity (ε, %) was evaluated using the gravimetric method [2–4]. The weight of the membranes was utilized indirectly to predict the porosity of the as-prepared membranes using the **equation (S1)**.

$$\varepsilon\ (\%) = \left(\frac{\frac{(W_{wet} - W_{dry})}{\rho_W}}{\left(\frac{W_{wet} - W_{dry}}{\rho_W} + \frac{W_{dry}}{\rho_{CA}} \right)} \right) \times 100 \qquad \textbf{(S1)}$$

where ε represents the porosity in percentage (%), ρ_w and ρ_{CA} are densities of water (1 g/cm^3) and CA (1.5 g/cm^3), respectively, W_{wet} and W_{dry} represent the weight of the wet and dried membrane.

The shrinkage ratio was investigated by cutting the as-prepared membranes into a pre-determined area (17.35 cm^2) with a known length and thickness which were measured before and after dipping in deionized water for 24 h. The shrinkage of the membranes was calculated using **equation (S2):**

$$Shrinkage\ (\%) = 1 - \left(\frac{D_{dry} - T_{dry}}{D_{wet} - T_{wet}}\right) \times 100 \qquad \textbf{(S2)}$$

where D_{dry} and D_{wet} represent the diameter of the dry and wet membranes, respectively, and T_{dry} and T_{wet} represent the thickness of the dry and wet membranes, respectively.

The determination of the pore volume was evaluated using water uptake of the membranes by immersing dry membrane discs (diameter = 47 mm) in deionized water for 24 h. The wet membrane discs were wiped with blotter paper and weighed immediately. To determine the dry weight of the membranes, wet membranes were dried in an electric oven for 24 h at 75 °C and weighed thereafter [5,6]. The water uptake was calculated using **equation** (**S3**):

$$\text{Water uptake } (\%) = \frac{W_{wet} - W_{dry}}{W_{wet}} \qquad \textbf{(S3)}$$

where W_{dry} and W_{wet} represent a dry and wet weight of the membrane disc, respectively.
These measurements were conducted as the porosity and thickness of the membrane in the presence of water tend to increase membrane swelling. An increase in porosity of the membrane signifies that there is high volume of pores per total volume of the membrane [7], hence, the membranes with porosity (%) over 80% are desired [8,9]. Moreover, porous photocatalytic membranes tend to exhibit high porosity due to their excess pore structures. Shrinkage ratio is performed by measuring wet and dry membranes thickness and length. After drying membranes tend to shrink and thickness and length of the membrane is reduced. Reports suggested that lower shrinkage ratio below 20-25% are desired. The filtration process of high shrinkage ratio hinders water permeation flux and the rejection of the contaminant, by squeezing or blocking the pore passages [9]

S10

Evaluation of the efficiency of the photocatalytic membrane

The photodegradation efficiency (PDE) of KP in solution were calculated using **equation (S4):**

$$PDE\ (\%) = (A_o - A_t)/A_o \times 100\% = (C_o - C_t)/C_o \times 100\% \qquad \textbf{(S4)}$$

where C_0 and A_0 are initial concentration and absorbance at t = 0 of the feed (KP), respectively. C_t and A_t are the concentration and absorbance at a certain time (t) of the filtrate solution, respectively. The initial concentration of 10 mg/L KP was utilized as the feed.

S11

Electrical energy consumption

Electrical energy consumption (E_{EC}) was calculated using **equation (S5):**

$$\text{Electrical energy consumption } (E_{EC}) = (P \times t)/(60 \times V \times k) \qquad \textbf{(S5)}$$

where P denotes the electrical power (kW), t represents the reaction time (h) and V is the volume (m^3), and *k* denotes the rate constant (min^{-1}).

S12

Table S1. The water quality characteristics of the different water matrixes used in this work

Characteristics	**Water type**		
	Distilled water	Drinking water	Groundwater
TOC, ppm	0.05	0.71	0.77
Total hardness (mg	72	252	254
pH	5.8	7.7	7.9
UV (254 nm)	0	0.06	0.07
Conductivity µS/cm	0.9	756	820
pH	5.9	7.8	7.9

S13

FTIR analyses

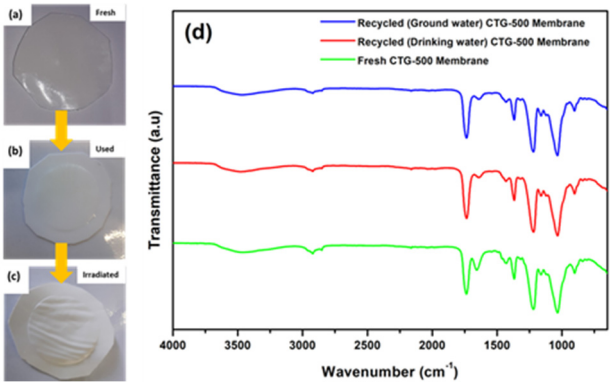

Figure S5. (a, b, and c) Series of steps for recycling the membranes and (d) ATR-FTR spectra of fresh CTG-500 membrane and after several cycles.

S14

Proposed degradation pathway of KP

The photodegraded fragments and intermediates were determined based on the measured mass-to-charge (m/z) ratio retrieved from LabSolutions software (Shimadzu, Japan). The uncatalyzed and photodegraded KP chromatograms at 0 and 5 h are presented in **Figure 13** (**a** and **b**), respectively. The uncatalyzed KP exhibited a single fragment at the retention time (R_t) of 3.094 min. The photodegraded KP using CTG-500 photocatalytic membrane showed 5 major fragments on the chromatogram including the parental peak appearing at R_t = 3.088 min. The other four fragments appeared at R_t = 1.534, 1.733, 2.933, and 3.675 min.

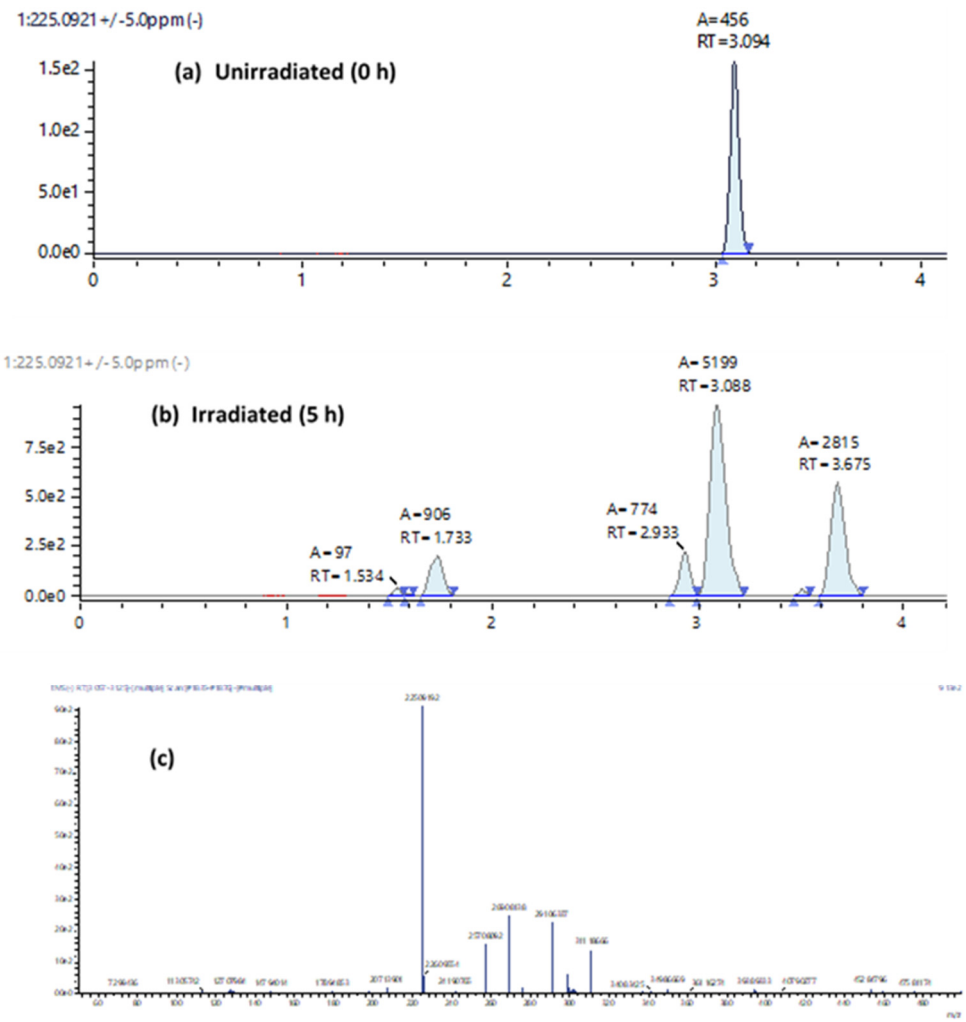

Figure S6. Chromatograms of (**a**) uncatalyzed and (**b**) photodegraded KP after 5 h; (**c**) mass spectrum for a peak at retention time 3.09 min.

The identification of the by-products was determined from the mass spectra analysis (Figure 13c). Figure 14 shows the proposed photodegradation pathway with the main by-products identified in Table 4. The major by-products which were identified on the mass spectra include (3-ethylphenyl)(phenyl)methanone (m/z = 209), [3-(1-hydroxyethyl)phenyl](phenyl)methanone (m/z = 240), 1-(3-benzolphenyl)ethan-1-one (224), 1-{3-[hydroxyl(phenyl)methyl]phenyl}ethan-1-ol (241) and [3-(1-hydroperoxyethyl)phenyl](phenyl)methanone (242) [10]. Upon visible light irradiation on the solution containing KP, under acidic media, KP is deprotonated to form intermediate (A) and rapidly converted into the intersystem crossing (ISC) to generate photoexcited triplet KP state (^{3}KP) as shown on intermediate (B) (Figure 14). The formation of the by-product (D) arose

from the decarboxylation of triplet state KP, forming carbanion (C) and subsequent protonation formed (3-ethylphenyl)(phenyl)methanone [11].

Biradical KP intermediate on carbanion and benzophenone can interact with dissolved molecular O_2 and further protonation on the peroxyl group would form a stable by-product (G). Further photoexcitation on (E) followed by the removal of water yield biradical and ISC KP, further molecular rearrangement produces a stable by-product (F). The elimination of water on the peroxyl group (G) and alpha-carbon forms anionic oxygen, further protonation on the oxygen group from the protons in the solution forms a hydroxyl group (E) [12].

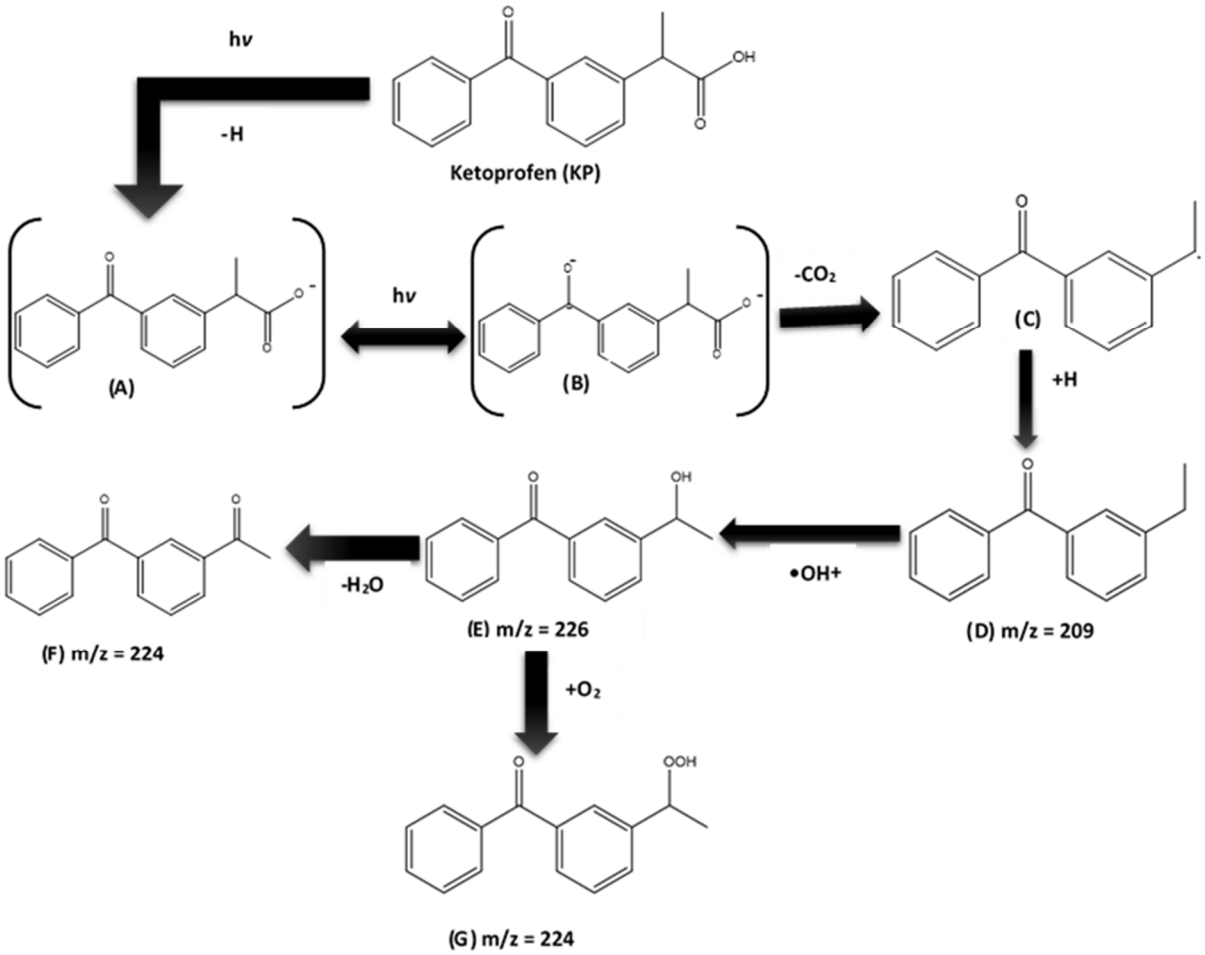

Figure S7. Proposed photodegradation pathway and the intermediates of KP.

References

[1] Q. Shi, G. Ping, X. Wang, H. Xu, J. Li, J. Cui, H. Abroshan, H. Ding, G. Li, CuO/TiO 2 heterojunction composites: an efficient photocatalyst for selective oxidation of methanol to methyl formate, Journal of Materials Chemistry A. 7 (2019) 2253–2260.

[2] V. Vatanpour, S. Faghani, R. Keyikoglu, A. Khataee, Enhancing the permeability and antifouling properties of cellulose acetate ultrafiltration membrane by incorporation of ZnO@ graphitic carbon nitride nanocomposite, Carbohydrate Polymers. 256 (2021) 117413.

[3] W. Li, B. Li, M. Meng, Y. Cui, Y. Wu, Y. Zhang, H. Dong, Y. Feng, Bimetallic Au/Ag decorated TiO2 nanocomposite membrane for enhanced photocatalytic degradation of tetracycline and bactericidal efficiency, Applied Surface Science. 487 (2019) 1008–1017.

[4] M.A. Mohamed, W.N.W. Salleh, J. Jaafar, A.F. Ismail, M. Abd Mutalib, N.A.A. Sani, S. Asri, C.S. Ong, Physicochemical characteristic of regenerated cellulose/N-doped TiO2 nanocomposite membrane fabricated from recycled newspaper with photocatalytic activity under UV and visible light irradiation, Chemical Engineering Journal. 284 (2016) 202–215.

[5] S.D. Neelapala, A.K. Nair, P.E. JagadeeshBabu, Synthesis and characterisation of TiO2 nanofibre/cellulose acetate nanocomposite ultrafiltration membrane, Journal of Experimental Nanoscience. 12 (2017) 152–165.

[6] R. Abedini, S.M. Mousavi, R. Aminzadeh, A novel cellulose acetate (CA) membrane using TiO2 nanoparticles: preparation, characterization and permeation study, Desalination. 277 (2011) 40–45.

[7] P.G. Ingole, K.H. Kim, C.H. Park, W.K. Choi, H.K. Lee, Preparation, modification and characterization of polymeric hollow fiber membranes for pressure-retarded osmosis, RSC Advances. 4 (2014) 51430–51439.

[8] Y.H. Cho, J. Han, S. Han, M.D. Guiver, H.B. Park, Polyamide thin-film composite membranes based on carboxylated polysulfone microporous support membranes for forward osmosis, Journal of Membrane Science. 445 (2013) 220–227.

[9] L.A. Shah, T. Malik, M. Siddiq, A. Haleem, M. Sayed, A. Naeem, TiO2 nanotubes doped poly (vinylidene fluoride) polymer membranes (PVDF/TNT) for efficient photocatalytic degradation of brilliant green dye, Journal of Environmental Chemical Engineering. 7 (2019) 103291.

[10] S. Miao, H. Zhang, S. Cui, J. Yang, Improved photocatalytic degradation of ketoprofen by Pt/MIL-125 (Ti)/Ag with synergetic effect of Pt-MOF and MOF-Ag double interfaces: Mechanism and degradation pathway, Chemosphere. 257 (2020) 127123.

[11] C. Martínez, S. Vilariño, M.I. Fernández, J. Faria, J.A. Santaballa, Mechanism of degradation of ketoprofen by heterogeneous photocatalysis in aqueous solution, Applied Catalysis B: Environmental. 142 (2013) 633–646.

[12] L. Hykrdová, O. Bajt, J. Jirkovský, Mechanism and kinetics of photochemical transformation of ketoprofen and its degradation intermediates, Journal of Hazardous Materials. 353 (2018) 70–79.